CORE DENSITY PEAKING EXPERIMENTS IN JET, DIII-D AND C-MOD IN VARIOUS OPERATIONAL SCENARIOS – DRIVEN BY FUELING OR TRANSPORT?

T. TALA, A. SALMI
VTT
Espoo, Finland
Email: Tuomas.tala@vtt.fi

S. MORDIJCK
The College of William and Mary
Williamsburg, USA

H. NORDMAN, F. ERIKSSON, E. FRANSSON, M. OBERPARLEITER, A SKYMAN, P. STRAND, D. TEGNERED
Chalmers University of Technology
Göteborg, Sweden

C. BOURDELLE
CEA, IRFM
Saint-Paul-lez-Durance, France

J. CITRIN
DIFFER
Eindhoven, Netherlands

A.CZARNECKA
IPPLM
Warsaw, Poland

C. GIROUD, J. HILLESHEIM, C. MAGGI, M. MASLOV, S. MENMUIR,
CCFE
Abingdon, UK

A.HUBBARD, J.W. HUGHES, E. TOLMAN
MIT Plasma Science and Fusion Center
Cambridge, USA

P. MANTICA, A. MARIONI
Istituto di Fisica del Plasma
Milano, Italy

G. MCKEE
University of Wisconsin - Madison
Madison, USA

L. MENESES, M. TSALAS
ITER Organisation
Cadarache, France

V. NAULIN
Technical University of Denmark, DTU, Physics Department
Lyngby, Denmark

C. PETTY
General Atomics
San Diego, USA

T. RHODES
University of California
Los Angeles, USA

G. SIPS
EU Commission
Brussels, Belgium

H. WEISEN
SPC, CRPP
Lausanne, Switzerland

AND JET CONTRIBUTORS*
*See the author list of "X. Litaudon et al 2017 Nucl. Fusion 57 102001

Abstract. Core density profile peaking and electron particle transport have been extensively studied by performing several dimensionless collisionality (υ*) scans in various plasma operation scenarios on JET and on DIII-D and a 2-point υ*scan in I-mode on C-Mod. This is the first time when electron particle transport coefficients in H-mode have been measured in tokamaks with high resolution diagnostics and thus, we are in a position to distinguish between the NBI source and inward pinch in contributing to density peaking. In JET, the NBI particle source is contributing 50-60% to the peaking in plasmas where T_e/T_i~1 and at υ*=0.1-0.5 (averaged between r/a=0.3-0.8) independent of υ*. On DIII-D, the density peaking is dominantly a transport effect (inward pinch) at low υ* while the NBI contributes to density peaking around 30-40% at higher υ*. These dimensionless υ* scans give the best data for model validation. TGLF simulations are in fairly good agreement with the experimental results with respect to the role of NBI versus inward pinch in JET and with high υ* discharge on DIII-D. GENE predicts larger role for the NBI fueling in JET than observed in experiment, but qualitatively agrees on the large role of NBI fueling in peaking the density profile. GENE is in fair agreement within the DIII-D scan with respect to the experimental result on the relative weight of NBI fueling versus inward pinch. Overall the various modelling gives fairly good confidence to use these models/codes in predicting density peaking at least in higher υ* plasmas. In L-mode plasma conditions, the role of the NBI source is small, typically 10-20% and the electron particle transport coefficients are large. On C-Mod, the I-mode density peaking database indicated that in the I-mode plasmas, there is no υ* dependence in density peaking. This result indicates that particle transport characteristics are more analogous to those of L-mode than H-mode and similar to L-mode ones observed in JET and DIII-D.

1. INTRODUCTION

Electron and ion particle transport due to its complexity in tokamaks has received much less attention than heat transport channels. Therefore, the respective role of particle transport versus fueling in affecting the density peaking in ITER is not well understood [1]. The shape of the density profile has a significant influence on fusion performance and impurity transport.

Earlier database studies in JET, AUG, C-Mod etc showed that density peaking scales with several plasma parameters, the most dominant ones being collisionality υ*, Greenwald fraction and NBI fuelling [2,3]. Collisionality was found to be the dominating parameters in JET, and this was further supported in C-Mod experiment where the core fueling is small [4]. The neutral beam fuelling source was found to be the second most important factor. On the other hand in L-mode plasmas, the plasma internal inductance or the shape of the q-profile was to found to be the key factor in determining the density peaking [5]. While the database studies suggested the dominant role played by the collisionality in affecting density peaking, other particle transport analyses in JET emphasized the importance of the particle sources [6,7,8]. Modelling has already suggested that T_i/T_e has a significant effect on the peaking [9]. What complicates the analysis is that on JET, T_i/T_e and NBI source are strongly correlated, and at the same time have opposite effects on the density gradient/peaking. Therefore correlation between density peaking and the source has always seemed to be low and the role of NBI underestimated. To unambiguously estimate the relative roles of different factors affecting density peaking, one has to separate the effect of transport and fueling from each other and look into the parametric dependences of transport coefficients, by measuring the diffusion D and convection V.

Core density profile peaking is extensively studied by performing several dimensionally matched collisionality (υ*) scans in various plasma operation scenarios on JET as well as by executing a 3-point υ* scan on DIII-D and a 2-point I-mode υ* scan on C-Mod. Gas puff modulation technique has been developed with high quality time-dependent density profile measurements to determine particle transport coefficients on JET and DIII-D [10,11]. A key focus is to determine the relative importance of inward convection versus NBI particle source in creating the observed core density peaking.

2. THE DIMENSIONLESS COLLISIONALITY SCANS WITH GAS PUFF

The following four 3-point υ* scans were performed in JET: (i) high power ELMy H-mode featuring low β, (ii) hybrid like high β H-mode plasma, (iii) ELMy H-mode plasma in Hydrogen and (iv) L-mode with Carbon wall. The dimensionless parameters, q, ρ^*, β_n and T_i/T_e were typically matched very well while υ* is varied by a factor of 5. The density profiles, measured with Thomson scattering diagnostics from the four scans are shown in fig. 1 (left). A similar 3-point υ* scan in ELMy H-mode, but at lower υ* (the υ* ranges are shown in figure (2) and Table 1) was executed on DIII-D in figure 1 (right). Density peaking increased with decreasing υ* very similarly to JET.

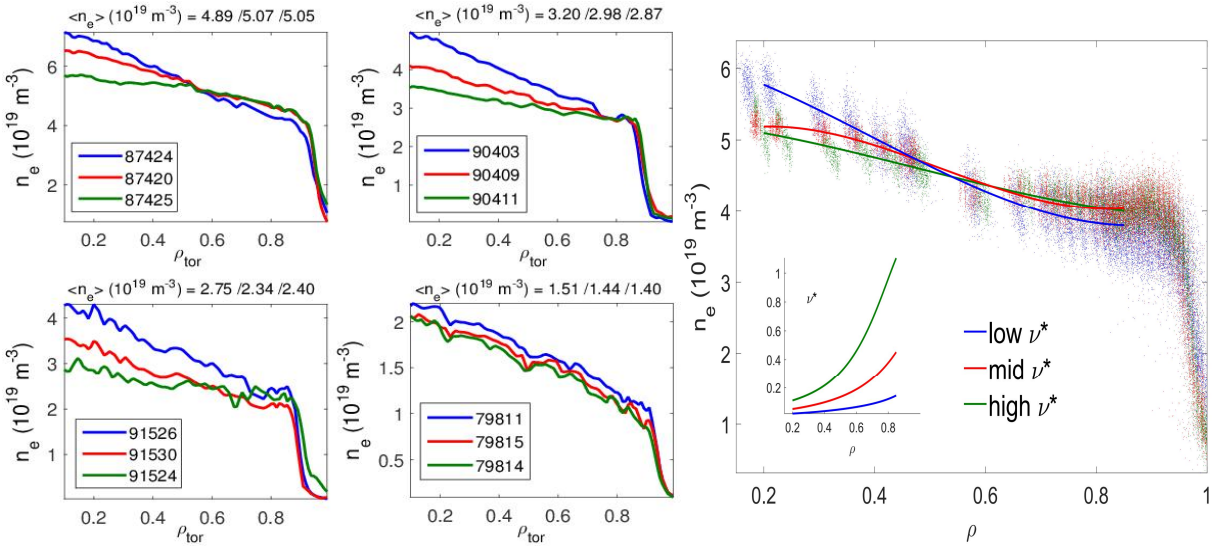

Figure 1. Left: Density profiles from the following four dimensionless υ* scans: (top left, case (i)) ELMy H-mode featuring low β, (top right, case (ii)) hybrid like high β plasma, (bottom left, case (iii)) ELMy H-mode plasma in Hydrogen and (bottom right, case (iv)) L-mode. Right: ELMy H-mode υ* scan from DIII-D . The blue colour refers to the low υ* case, the green one to high υ* (red intermediate). The numbers on top indicate the volume averaged densities, in the order blue, red, green.

The dimensionless parameters, q, ρ^*, β_n and T_i/T_e (being very close to 1 in each of the scans in JET and around 1.3 in DIII-D) were typically matched very well, the difference between the shots being only a few % (<10% in worst case). The temperature gradient length R/L_T was constant within the scan in JET, but on DIII-D the low υ* shot has larger R/L_{Ti} in the outer core smaller in the centre. The rotation and Mach number were not matched well in JET (increases with NBI power), on DIII-D with counter beams this match is better. The is some evidence that E × B shear from the toroidal rotation, not kept constant within these scans, can increase density peaking.

3. EXPERIMENTAL PARTICLE TRANSPORT COEFFICIENTS

Gas puff modulation technique has been developed and optimized to study core particle transport and core particle sources in JET [10] and on DIII-D [11]. Typically gas puff modulation experiments were performed with a gas valve at the top of the machine at 3-5Hz frequency using a rectangular waveform. The local electron density response to the gas injection was measured with either a multi-band density profile reflectometer capable of good spatial and temporal resolution or High Resolution Thomson Scattering (HRTS) diagnostics or both in each device close to the outer midplane. Density modulation amplitudes below 1% (in the core) are reliably measured thus allowing minimal plasma disturbance and the possibility to use data also from multiple harmonics.

The analytical expressions for the diffusion coefficient D and particle pinch V are obtained from the approach based on perturbative particle transport equation, modulated density data and stationary background transport [12]. The equations are modified to include the real geometry. In the case of DIII-D, the convection is calculated from the particle flux equation instead of the formula in Ref. [11] once the diffusion D is obtained from [12]. The neutral particle source over the separatrix is negligible inside $\rho<0.8$ or even $\rho<0.9$.

The experimental D and V (averaged from $\rho=0.5$ to $\rho=0.8$) values are shown in figure 2. The D and V vary within this radial range, but to present them in one figure, averaged values are used. In the L-mode υ* scan (lower row), D and V are large in all cases even if the NBI power is much smaller than in the H-mode cases (upper row). This is suggesting that in L-mode, the role of NBI fueling is small. On the other hand, in H-mode (case (i) in JET and DIII-D υ* scan in figure 1), the transport coefficients, both D and V, are small (except the low υ* DIII-D case) though V is increasing with decreasing υ* and D increases with NBI power. As particle transport is small in the H-mode plasmas (except low υ* DIII-D shot), the NBI source could be expected to be quite an important factor contributing to the density peaking.

The transport coefficients determined from the modulated density represent the perturbative transport coefficients, which may not necessarily correspond to the power balance ones. To study this more thoroughly, stand-alone TGLF runs to scan the particle flux as a function of the inverse density gradient length were performed both in JET and DIII-D around the experimental plasma parameters. This analysis shows that the flux gradient curve is almost linear in JET, indicating that the perturbative transport coefficients represent well the power balance ones. The dependence is not as linear in the case of the DIII-D, giving a possiblility that the power balance D is not necessarily the same as the perturbative one D_{pert}. Another independent experimental study to this one was carried out using the relation of D_{pert} and D_{pb} and the conclusion there was that while for the high and medium υ* the ratio is close to 1, it departs from 1 at low υ*, in the same way as shown by TGLF analysis. The higher measured transport may be related to the observed increase in the low k turbulence, measured with BES, with decreasing υ*.

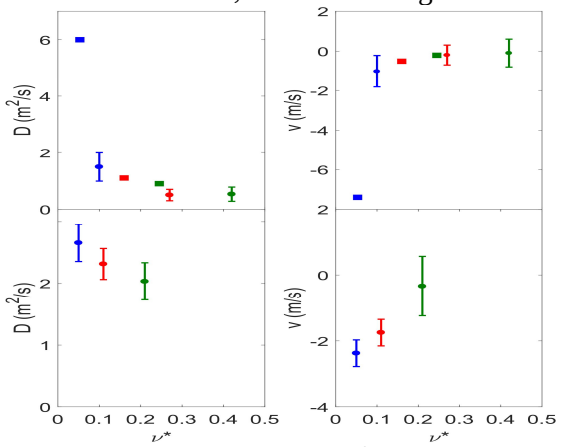

Figure 2. The experimental D and V for the both JET and DIII-D H-mode scans in upper row and in lower row for the JET L-mode scan. Colours corresponds to the pulses as in figure 1. The JET points are denoted by the dots with error bars and the DIII-D points by the squares. The transport coefficients are averaged from $\rho=0.5$ to $\rho=0.8$.

4. TRANSPORT MODELLING AND GYRO-KINETIC ANALYSIS OF DIMENSIONLESS υ* SCANS

Extensive transport simulations with JETTO transport code [13] have been performed to study the physics of particle transport, with the particular emphasis on understanding the origin of the density peaking. TGLF transport model [14] has been used to simulate all the 4 dimensionless υ* scans in JET and H-mode υ* scan in DIII-D. The simulation results from the baseline H-mode scans from each device are illustrated in figure 3. The temperature predictions are in good agreement with the experiment for all JET cases (left frames) and also for the DIII-D cases except the low υ* case (upper row) where T_i is significantly overpredicted in the region of interest at $0.5 < \rho < 0.8$. The density profile is very well predicted by TGLF in each case when the NBI particle source is taken into account. The relative role of the NBI particle source can be seen in the simulations without the NBI source (red dashed lines). According to TGLF, the NBI contributes around 50% to density peaking in JET and around 50-80% on DIII-D (the fractions are shown in figure (5)). However, the density prediction for the DIII-D low υ* case (predicted T_i in disagreement) should be taken with great care as the role of NBI would be only around 20% if the experimental temperatures are used in the simulation (only n_e predicted), and the good agreement with fully predictive simulation fortuitous.

The same conclusion as for JET H-mode scan is also obtained for the JET Hybrid scenario scan and the the ELMy H-mode scan in Hydrogen plasma (not shown here), i.e. TGLF assigns the dominant role for the NBI particle source over the inward pinch in contributing to the density peaking.

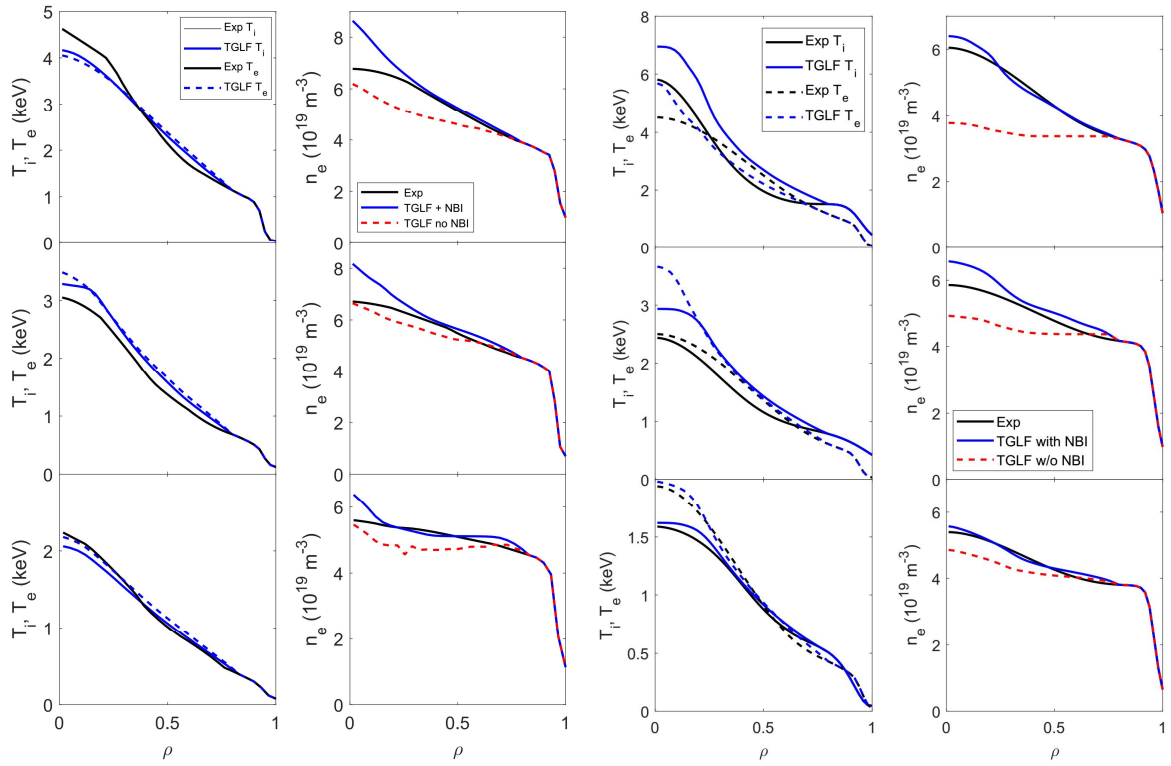

Figure 3. JETTO transport simulations with TGLF model for the JET (two left frames) and DIII-D (two right frames) ELMy H-mode scans. The upper row corresponds to the low υ* discharges, the middle one to the intermediate υ* cases and the lower one to the high υ* cases. Note that experimental T_i=T_e in JET.

Gyro-kinetic GENE simulations were performed to infer the peaking factor (R/L_n= -Rv/D) of the background electrons at zero flux at various radii. The linear and nonlinear simulations of ITG/TEM mode turbulence were performed in flux tube domain, with a realistic geometry, including finite β_e effects and collisions using a Landau-Boltzmann collision operator, but excluding fast particles and impurities.

The GENE simulation results for the JET L-mode and H-mode JET dimensionless υ* scans (upper row) are shown in figure 4. Peaked density profiles are obtained for L-mode, and GENE predictions are consistent with the experimental density peaking. In H-mode, while the experimental density profiles are peaked, GENE predicts flat profiles for low υ* discharge and hollow density profiles for higher υ* values for each scan at ρ=0.6. Similar predictions (not shown here) are seen for the Hybrid

and Hydrogen H-mode scans. As a consequence, the GENE results give larger emphasis on the contribution of NBI fueling in contributing to the density peaking in JET. On DIII-D, GENE agrees with the experimental results, i.e. virtually all density peaking is originating from the pinch at low υ* and large fraction also at higher υ* (depends on $k_\theta\rho_s$). The stand-alone TGLF is in good agreement with GENE and experiment on the origin of the peaking. This confirms the experimental obervation that JET and DIII-D are different with respect to the source of density peaking in particular at low υ*.

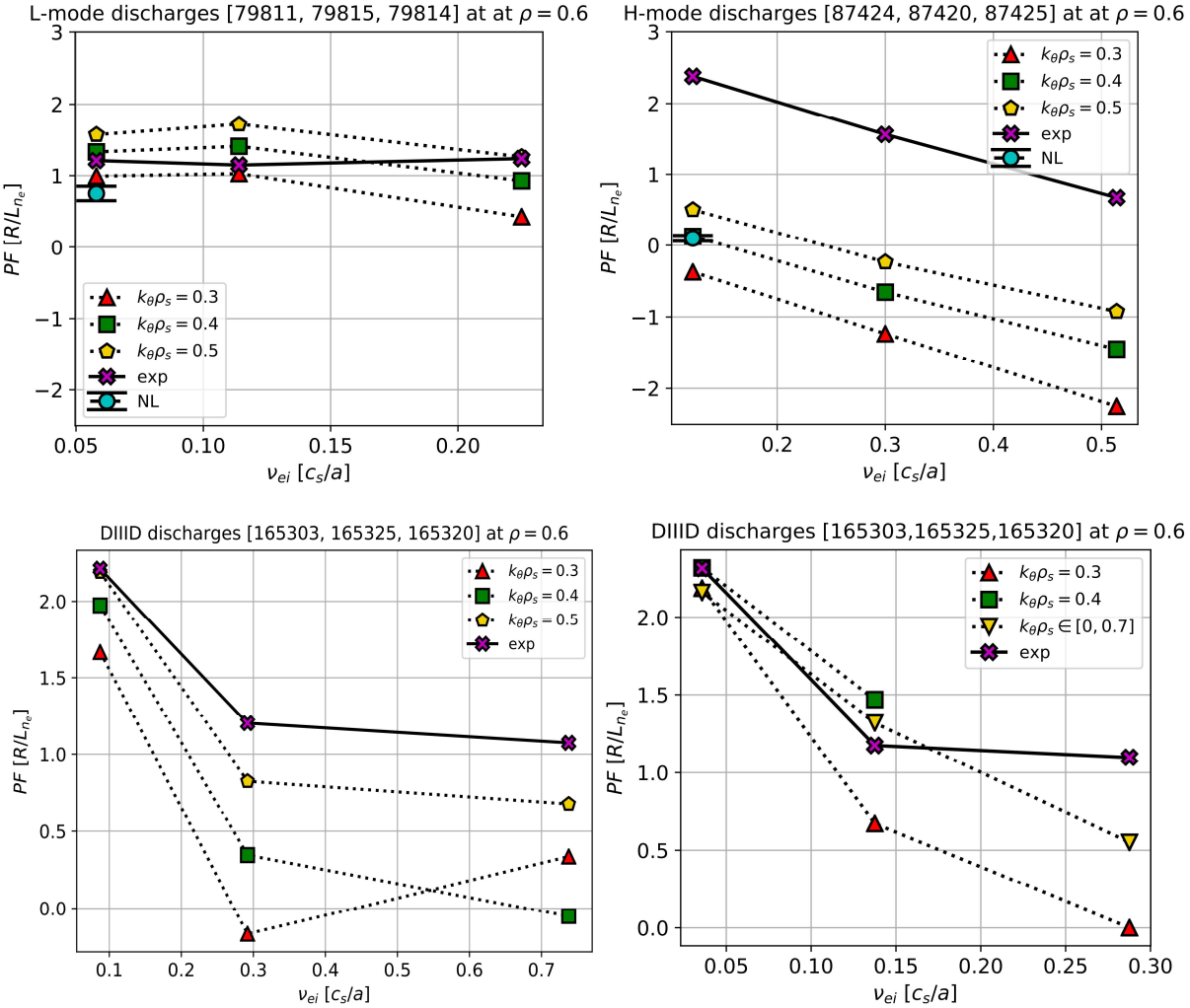

Figure 4. GENE simulations of density peaking factors (PF) for the JET L-mode (top left), H-mode (top right) as well as the DIII-D (bottom left) dimensionless υ* scans at various k_θ values, including one non-linear run per shot, all simulations at ρ=0.6. Bottom right: As in bottom left, but with using stand-alone TGLF instead of GENE.

5. ANALYSIS OF THE VARIOUS CONTRIBUTORS TO THE DENSITY PEAKING IN THE υ* SCANS

The key question to understand in the core electron particle transport is what fraction the inward convection versus what fraction the NBI particle source has in contributing to the observed density peaking. And further what are its parametric dependences, in particular with decreasing υ*. It is important to note that the NBI fueling rate increases, for example in the high power JET H-mode υ* scan, from 0.8×10^{21} 1/s to 2.3×10^{21} 1/s while density peaking increases by a factor of 3 and υ* decreases simultaneously by a factor of 5.

To quantify the core density peaking, the following definition has been used as the figure of merit: $(n_e(0.5) - n_e(0.8))/n_e(0.8)$. The region is motivated by the availability of the experimental D and V on that region, outside the edge neutral source may play a role and inside the density modulation is either too small or sawtooth and other factors may make the analysis more complicated. The results are shown in figure 5 for the JET and DIII-D H-mode scans (left) and JET L-mode scan (right). The blue points have been obtained from the particle transport simulations where the experimentally determined

D and V (figure 2) have been used as the transport coefficients from ρ=0.5 up to ρ=0.8 (nothing else included), but without the NBI particle source. Therefore, the part below the blue points represent the contribution of the transport (in practice the influence of inward pinch V) to the total density peaking (black symbols). And correspondingly, the part between the black and blue symbols represent the contribution of the NBI particle source to the density peaking. For example, the lowest υ* discharge on DIII-D has more than 90% of the peaking originating from transport (pinch) as the blue diamond is almost as high as the black diamond. The TGLF points are obtained in the same way, i.e. the area below the red symbols show the relative contibution from the transport with respect to total peaking (black symbols), simulated without the NBI particle source. And the difference between the black and red symbols mark the TGLF predictions for the relative contribution from the NBI source to the density peaking. The key data of the discharges presented in figure 5, including the peaking factors, are listed in Table 1.

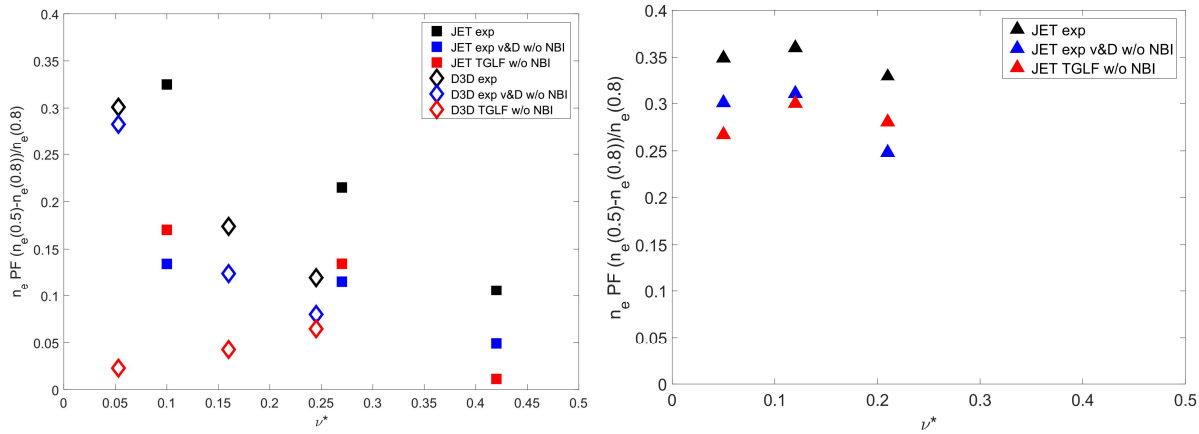

Figure 5. Relative contributions of the inward particle pinch and NBI particle source to the electron density peaking for JET and DIII-D H-mode scans (left) and JET L-mode scan (right). The area below the blue (experimental) and red (TGLF) symbols mark the fraction of inward pinch on peaking and the area between the black and red or blue symbols the one of NBI fueling.

Table 1. The key parameters and peaking numbers for the JET and DIII-D H-mode scans, JET L-mode scan and typical parameters for the C-Mod I-mode discharges.

Pulse No.	Machine	Type	Collisionality	PF ne(0.5)-ne(0.8)/ne(0.8)		PF	PF	PF
				Experiment	Exp D and V, w NBI	Exp D and V, w/o NBI	TGLF w NBI	TGLF w/o NBI
87424	JET	H-mode	0.1	0.325	0.29	0.12	0.351	0.184
87420	JET	H-mode	0.27	0.216	0.346	0.187	0.25	0.157
87425	JET	H-mode	0.42	0.106	0.151	0.07	0.08	0.001
165303	DIII-D	H-mode	0.053	0.301	0.313	0.294	0.29	0.022
165325	DIII-D	H-mode	0.16	0.174	0.176	0.126	0.204	0.05
165320	DIII-D	H-mode	0.245	0.12	0.122	0.079	0.13	0.07
79811	JET	L-mode	0.05	0.349	0.477	0.411	0.392	0.3
79815	JET	L-mode	0.12	0.36	0.29	0.25	0.42	0.35
79814	JET	L-mode	0.21	0.329	0.11	0.083	0.386	0.329
	C-Mod	I-mode	0.02	0.3				

The JET H-mode υ* scan (squares) shows that the experimentally determined D and V (blue squares) contribute around 40-50% to the density peaking for each υ*, leaving the fraction 50-60% to the NBI particle source. TGLF agrees on these numbers remarkably well except for the high υ* shot it predicts around 90% contributions from the NBI. The DIII-D H-mode scan is different to large extent as the experimental D and V would be responsible for about 60-70% of the peaking at high υ* and almost 100% at low υ*. There is a clear trend in the experimental data (blue symbols) that the role of the NBI source in contributing to the density peaking is smaller on DIII-D than on JET in H-mode plasmas. As discussed earlier, the temperature predictions are not in agreement in the low υ* case and therefore, one should not trust even the density prediction. In fact, with prescribed temperature, TGLF gives the opposite result, i.e. most peaking is due to inward pinch, and this is also seen in figure 4 in the TGLF stand-alone simulations. In the JET L-mode υ*scan, 80-90% of the peaking originates from the transport, both the experimental data and TGLF simulations agreeing on this well.

6. DENSITY PEAKING IN HIGH AND LOW T_E/T_I JET PLASMAS

To further study the density peaking in other JET plasmas at different T_e/T_i, TGLF modelling has been performed for non-fuelled H-mode plasma at 8 MW of ICRH power and a high power hybrid scenario at higher β_N than the ones achieved in the dimensionless υ* scans. The simulation results are shown in figure 6. The ICRH only pulse (upper row) has high T_e/T_i~1.5 at midradius, but still without NBI, density is peaked. TGLF predicts both temperatures and density peaking accurately, giving confidence on the overall capability of TGLF to predict density peaking correctly under quite varying plasma conditions. This is the first JET H-mode pulse where also GENE predicts peaked density profile in quantitative agreement with the experimental peaking (not shown here). For the high β_N hybrid scenario pulse T_e/T_i=0.7 (lower row), TGLF predicts density peaking also well, but in the simulation without the NBI source, most of the peaking is lost. Consequently, the same conlcusion holds here that the NBI source is the domninant contributor to the density peaking even at very low υ* if $T_e/T_i \leq 1.0$. The GENE simulations agree with TGLF also the high β_N JET hybrid pulse, most of density peaking is due to NBI. The peaking would increase with increasing T_e/T_i ratio significantly.

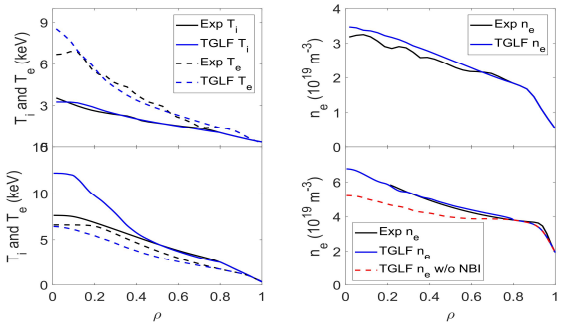

Figure 6. Transport simulation with TGLF model for the low β_N JET ICRH only discharge (upper row) and high β_N JET hybrid pulse (lower row).

7. DENSITY PEAKING IN NON-FUELLED C-MOD PLASMAS WITH I-MODE PLASMA EDGE

The dependence of density peaking on υ* was studied in I-mode on C-Mod. The C-Mod discharges do not have NBI fueling and therefore will give relevant information on the role of NBI fueling and a valuable comparison to JET and DIII-D υ* scans. Moreover, I-mode has special characteristics for edge particle transport with respect to H-mode. The steady-state n_e data indicates no dependence on υ* in I-mode as shown in figure 7. This is similar to JET and DIII-D L-mode dependence on υ*. This result indicates that particle transport characteristics are more analogous to those of L-mode than H-mode and similar to L-mode ones observed in JET and DIII-D. Gas puff modulation was also applied on C-Mod, but the modulated density data is too noisy to able to extract the particle transport coefficients.

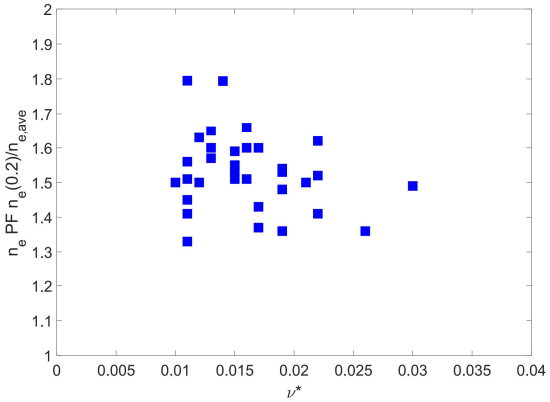

Figure 7, Density peaking of I-mode discharges at various plasma conditions on C-Mod as a function of υ*. The definition of peaking differs here from the one in figure 5.

8. CONCLUSIONS

This is the first time when electron particle transport coefficients have been measured in tokamaks with high resolution diagnostics. The role of NBI source in affecting density peaking has been found larger than expected in the various JET H-mode υ*scans. The NBI particle source is contributing 50-60% to the peaking in plasmas where T_e/T_i~1 and at υ*=0.1-0.5 and within this range, independent of υ*. TGLF simulations are in good agreement with the experimental results with respect to the role of NBI particle source versus inward pinch in density peaking. GENE predicts flat or hollow density profiles for JET H-mode plasmas, thus giving higher weight on NBI fueling than experimentally observed. For T_e/T_i~1.5 and low β_N H-mode conditions (no NBI source), both TGLF and GENE predicts correctly the peaked n_e profile.

The DIII-D results are dissimilar to JET with respect to density peaking. The inward pinch contributes 60-70% to the density peaking at high and medium υ*, up to 90% at low υ*, with the caveat of that we may overestimate the power balance transport coefficients by assuming them to be equal to the perturbative ones and thereby, underestimate the role of NBI fueling. GENE predictions are in good agreement with the experimental results with respect to density peaking, and this is further supported by stand-alone TGLF simulations. The turbulence measurements show that low k turbulence is increasing with decreasing υ* while $k_\theta\rho_s$=1-5 turbulence increases with increasing υ*.

In L-mode plasma conditions, the role of the NBI source is small, typically 10-20%. On C-Mod, the I-mode density peaking database indicated that the I-mode particle transport characteristics are similar to those of L-mode, i.e. no dependence of density peaking on υ* was found.

The predictive capability of TGLF is quite convincing here with various experimental results provided that the temperatures are predicted accurately enough. With disagreeing temperature predictions, the density predictions are not satisfactory. GENE simulations are also qualitatively agreeing with experimental results in most conditions, although GENE tends to underestimate the effect of the pinch on density peaking at T_e/T_i~1 conditions.

In conclusion, density peaking between JET (NBI fueling dominant) and DIII-D (transport dominant) originates from different sources especially when going to low υ*. To answer the question in the title of this paper, we can compare the simulations of the JET and DIII-D H-mode discharges – the DIII-D discharges of this υ* scan are in a different turbulence regime where the Trapped Electron modes (TEM) play a stronger role. This appears to be due to the lower υ*, higher magnetic shear and larger R/L_{Te} in the DIII-D scan than in the JET one. These all tend to increase the density peaking. Further work, including nonlinear GENE simulations, is needed in order to investigate their individual contributions to the difference between JET and DIII-D. The key question unanswered is what happens in JET conditions when one moves to lower υ*; whether the high density peaking without the NBI source will take place or not. The lesson learned is that in order to be able to predict the density peaking well, one needs to know the plasma regime well, and this is certainly true when extrapolating to future devices. TGLF and GENE seem both relatively well to be able to predict density peaking in various plasma conditions. The electron density peaking with different isotopes and extension of the parameter scans will be the scope of future experimental work to consolidate ITER and DEMO predictions.

ACKNOWLEDGEMENTS

"This work has been carried out within the framework of the EUROfusion Consortium and has received funding from the Euratom research and training programme 2014-2018 under grant agreement No 633053. The views and opinions expressed herein do not necessarily reflect those of the European Commission. This material is based upon work supported by the Department of Energy under Award Number DE-FC02-04ER54698. Supported by U.S. Department of Energy awards DE-FC02-99ER54512, DE-SC0007880 and DE-SC0014264 using Alcator C-Mod, a DOE Office of Science User Facility. DIII-D data shown in this paper can be obtained in digital format by following the links at https://fusion.gat.com/global/D3D_DMP. This work was conducted under the auspices of the ITPA Topical Group on Transport and Confinement."

REFERENCES

[1] A. Loarte *et al*., Nucl. Fusion **53**, 083031 (2013).
[2] H. Weisen *et al.*, Plasma Phys. Control. Fusion **48**, A457 (2006).
[3] C. Angioni *et al*., Nucl. Fusion **47** 1326–1335 (2007).
[4] M. Greenwald *et al*., Nucl. Fusion **47** L26–L29 (2007).
[5] H. Weisen *et al*, Plasma Phys. Control. Fusion **46**, 751 (2004).
[6] M. Valovic *et al.*, Phys. Control. Fusion **46**, 1877 (2004).
[7] L. Garzotti *et al.*, Nucl. Fusion **46**, 994 (2006).
[8] M. Valovic *et al.*, Nucl. Fusion **47**, 196 (2007).
[9] M. Maslov *et al.*, Nucl. Fusion **49**, 075037 (2009).
[10] T. Tala *et al.*, 44th EPS Conf., Belfast, UK, (2017).
[11] S. Mordijck *et al.*, Nucl. Fusion **55**, 113025 (2015).
[12] H. Takenaga *et al.*, PPCF **40**, 193 (1998).
[13] M. Romanelli, *et al.*, Plasma and Fusion Research **9**, 3403023 (2014).
[14] G. Staebler *et al*. Phys. Plasmas **12**, 102508 (2005).